Numerical Investigation on the Motion of Free-Floating Crystals During DC Casting of Aluminum Alloys

Qipeng Dong, Hiromi Nagaumi, Haitao Zhang, Tianpeng Qu, and Jingkun Wang

Abstract

Macrosegregation formed during direct chill (DC) casting of aluminum ingots will deteriorate the mechanical property of products. The characteristic of macrosegregation is reported to be affected by the free-floating crystals, which was proved to result in the center negative segregation. The motion of free-floating crystals in ingots is numerically simulated. The model is developed to incorporate fluid flow, heat transfer, and the motion of free-floating crystals basing on the mixture model and Lagrangian approach. Efforts are made to investigate the motion of free-floating crystals in liquid and slurry zones during solidification of casting process. In addition, distribution of the dendrites in mush and solidified zones is also studied. The variation of macrosegregation with the influence of free-floating crystals can be primarily clarified according to the results.

Keywords

Numerical simulation • Free-floating crystals • Aluminum alloys • DC casting

Introduction

Macrosegregation formed during alloys solidification will significantly deteriorate the mechanical property of products. In DC-cast billets and ingots, movement and sedimentation/growth of free-floating crystals in the slurry zone is considered one of the main mechanisms of macrosegregation. Transport of free-floating crystals as considered being solute-lean crystals within the slurry zone by gravity and buoyancy forces, convective or forced flows accounts for the formation of inverse segregation. This theory was not accepted until 1980s [1], when the duplex structure characterized by a mixture of fine-branched dendrites and coarse-cell dendrites was observed near the ingot centerline by numerous experiments [2, 3]. Microsegregation measurements performed by Nadella et al. [4] showed that independent of grain refinement, coarse dendrite branches have a depleted concentration plateau in contrast to the fine dendrite arms, which substantiate the concept of solute-depleted floating crystals contributing to the centerline segregation.

Vreeman et al. [5, 6] developed a numerical model to investigate the effect of free-floating crystals and convection on macrosegregation in DC cast aluminum alloys. The velocity of free-floating crystals was assumed to be equal to the average solid and liquid interfacial velocity on the basis of the work of Ni and Incropera [7, 8]. Numerical results show that the negative segregation at the centerline increased with an increase in the packing fraction at which free-floating crystals are presumed to coalesce into a rigid dendritic structure. Using the method, Krane [9] evaluated the effect of the motion of free-floating crystals on the final macrosegregation patterns in a Pb-Sb-Sn alloy. Lesoult [10] pointed out that only moderate flux density of the floating crystals leads to the intense negative segregation, whereas the segregation was effectively reduced when a larger density of the floating crystals caused their early immobility. Reddy and Beckermann [11] predicted the commonly observed subsurface enrichment and depleted regions, as well as positive segregation at the centerline with a low grain density. With a higher grain density, negative segregation was predicted at the centerline. Turchin et al. [12] studied the

Q. Dong · H. Nagaumi (✉) · T. Qu
High-Performance Metal Structural Materials Research Institute, Soochow University, Suzhou, 215137, China
e-mail: zhanghai888jp@suda.edu.cn

H. Zhang
School of Materials Science and Engineering, Northeastern University, Shenyang, 110000, China

J. Wang
China Hongqiao Group Limited, Hong Kong, 256200, China

C. Chesonis (ed.), *Light Metals 2019*, The Minerals, Metals & Materials Series,
https://doi.org/10.1007/978-3-030-05864-7_38

solidification of an Al-4.5 pct Cu alloy in a shallow cavity under conditions of forced flow by fluid-dynamics simulations and experiments. In the study, they performed a particles-transport calculation in the flowing melt to simulate the settling of fragments in the beginning of the solidification process, and the fragments were modeled as spherical particles with the size 50 μm. The results indicate that the detached crystals or fragments could be transported by the fluid flow from the upstream part of the cavity and, finally, settle in the downstream corner, where the duplex (coarse and fine) internal structure can be observed. Another report by Eskin et al. [13] shows an obvious correlation between the negative segregation at the downstream section of the sample and the transport of solute-lean crystals by the flow. Currently, although we conclude that the floating crystals contribute to inverse segregation, doubts are expressed as to what extent the floating crystals could affect macrosegregation. Thus, the authors intend to perform some works to qualitatively describe how the free-floating crystals affect the macrosegregation patterns, as well as quantitatively analyze the influence of free-floating crystals on macrosegregation. Although previous studies indicate the correlation between negative segregation at centerline and the motion of free-floating crystals with fluid flow, the movement characters and distribution of free-floating crystals in DC cast billets are rarely reported. Therefore, as our initial work, the main purpose is to investigate the motion and distribution of free-floating crystals during DC casting process of aluminum alloys with a mathematic model, in which the fluid flow, solidification, and transport of free-floating crystals are simulated.

Model Description

Assumptions

(a) An incompressible Newtonian fluid was assumed and the effects of turbulence were approximated with the low Reynolds number turbulence model.
(b) Local thermodynamic equilibrium was assumed at the solid–liquid interface.
(c) The densities of liquid and solid were assumed to be constant and equal. Thus, the flow induced by shrinkage was not considered.
(d) The free-floating crystals are treated as spherical particles, ignoring the influence resulted from the variation of shape.
(e) A larger density (2700 kg/m^3) is adopted for the free-floating crystals in order to account for the effect of gravity.
(f) The growth and remelting of the free-floating crystals are not taken into account here.

Fluid Flow Model

Conservation Equations

The coupled model governing the conservation of mass, momentum, energy, and particle transport simultaneously valid in the liquid, mushy, and solid zones, can be expressed as follows.

Continuity Equation

$$\nabla \cdot (\rho \vec{u}) = 0 \tag{1}$$

where ρ and $\vec{u}$ represent mixture density and velocity, respectively, and they are defined using mass fractions f_n and volume fractions g_n for solid $(n = s)$ and liquid $(n = l)$ phases.

$$\vec{u} = f_s \vec{u}_s + f_l \vec{u}_l \tag{2}$$

$$\rho = g_s \rho_s + g_l \rho_l \tag{3}$$

In the present work, the volume fractions for solid and liquid are equal to the corresponding mass fractions as the same density assumed for the two phases.

Momentum Equation

$$\frac{\partial(\rho \vec{u})}{\partial t} + \nabla \cdot (\rho \vec{u}\vec{u}) = \nabla \cdot \left(\mu_{eff} \nabla \vec{u}\right) - \nabla p + \rho \vec{g} + S_u \tag{4}$$

where $\vec{u}_s$ represents the solid velocity, p is the pressure, and the effective viscosity μ_{eff} describing the sum of laminar and turbulent viscosity was defined to take into account the turbulence effect. The source term S_u can be described as follows:

$$S_u = \rho \vec{g} \beta_T (T - T_R) + \frac{(1 - f_l)^2}{f_l^3 + \xi} A_m (\vec{u} - \vec{u}_s) \tag{5}$$

where β_T represents the thermal expansion coefficient, T is temperature, the subscript R identifies the reference value, and ξ is a very small positive number.

The first term on the right-hand of Eq. (5) accounts for the thermal buoyancy, which resulted from the temperature gradient during solidification. The buoyancy term were calculated with the Boussinesq approximation. The second term represents the phase interaction force in the mushy zone, which was modeled as a porous medium wherein the

Darcy's law can be applied. A_m is permeability coefficient, which depends on the morphology of porous media.

Turbulence Model

To consider the effects of turbulence on the fluid flow, the low-Reynolds number $k-\varepsilon$ model [14, 15] was adopted here, which considered to be preferable than standard two-equation $k-\varepsilon$ model or high-Reynolds number $k-\varepsilon$ model in continuous casting processes. Governing equations of the model can be written as follows:

$$\frac{\partial k}{\partial t}+\nabla\cdot(\rho\vec{u}k)=\nabla\cdot\left[\left(\mu+\frac{\mu_t}{\sigma_k}\right)\nabla k\right]+G_k-\rho\varepsilon+\rho D+S_k \tag{6}$$

$$\frac{\partial \varepsilon}{\partial t}+\nabla\cdot(\rho\vec{u}\varepsilon)=\nabla\cdot\left[\left(\mu+\frac{\mu_t}{\sigma_\varepsilon}\right)\nabla\varepsilon\right]+C_1f_1G_k\rho\frac{\varepsilon}{k}-C_2f_2\rho\frac{\varepsilon^2}{k}+\rho E+S_\varepsilon \tag{7}$$

where k and ε are the turbulent kinetic energy and its rate of dissipation, respectively. S_k and S_ε represent the source terms for k and ε equations, which related to solidification as $S_k=\frac{1-f_l^2}{f_l^3+\xi}A_mk$, and $S_\varepsilon=\frac{1-f_l^2}{f_l^3+\xi}A_m\varepsilon$.

The turbulent viscosity can be calculated with the following equation:

$$\mu_t=\rho f_\mu C_\mu\frac{k^2}{\varepsilon} \tag{8}$$

The coefficients and empirical constants [15] used for the Launder–Sharma low-Reynolds number model are listed in Table 1.

Energy Equation

$$\frac{\partial(\rho H)}{\partial t}+\nabla\cdot(\rho\vec{u}H)=\nabla\cdot\left(k_{T,eff}\nabla T\right) \tag{9}$$

where $k_{T,eff}$ is the effective heat conductivity, which can be described as follows:

$$k_{T,eff}=\begin{cases}k_{T,l}+\frac{\mu_t}{\mathrm{Pr}_t}, & T\geq T_l\\ k_{T,s}f_s+k_{T,l}f_l, & T_s<T<T_l\\ k_{T,s}, & T\leq T_s\end{cases} \tag{10}$$

where $k_{T,l}$ and $k_{T,s}$ are the thermal conductivity of solid and liquid, respectively, and the turbulent Prandtl number Pr_t is listed in Table 1.

The enthalpy H in the energy conversation equation can be described as a function of temperature:

$$H=H_{ref}+\int_{T_{ref}}^{T}c_{ps}dT+f_lL \tag{11}$$

where c_{ps} is the specific heat, H_{ref} is the enthalpy at reference temperature T_{ref}, and L is the latent heat of fusion. In this work, the solid fraction was calculated with the Scheil equation, which expressed as [16]:

$$f_s=\begin{cases}0, & T\geq T_l\\ 1-\left(\frac{T_f-T}{T_f-T_l}\right)^{1/(k-1)}, & T_s<T<T_l\\ 1, & T\leq T_s\end{cases} \tag{12}$$

where T_l and T_s are the liquidus and solidus temperature respectively.

Particle Force Balance Equation

The motion of free-floating crystals is governed by the particle force balance equation defined as follows:

$$\rho_p\frac{\pi}{6}d_p^3\frac{\mathrm{d}\vec{u}_p}{\mathrm{d}t}=\vec{F}_{\mathrm{drag}}+\vec{F}_p+\vec{F}_b+\vec{F}_{\mathrm{VM}} \tag{13}$$

where ρ_p is the particle density, d_p is particle diameter ,$\vec{u}_p$ is particle velocity, $\vec{F}_{\mathrm{drag}}$ is particle drag force, $\vec{F}_p$ is pressure gradient force, $\vec{F}_b$ is buoyancy force, $\vec{F}_{\mathrm{VM}}$ is virtual mass force.

Drag force can be described as [17]:

Table 1 Coefficients and empirical constants used for the low-Reynolds number model

Parameters	Values	Parameters	Values
G_k	$\mu_t\left(\frac{\partial u_i}{\partial x_j}+\frac{\partial u_j}{\partial x_i}\right)\frac{\partial \mathbf{u}_i}{\partial \mathbf{x}_j}$	D	$2\mu\left(\frac{\partial(\sqrt{k})}{\partial x_i}\right)^2$
E	$2\frac{\mu\mu_t}{\rho}\left(\frac{\partial^2u_i}{\partial x_i\partial x_j}\right)^2$	f_μ	$\exp\left[-3.4/\left(1+\frac{\mathrm{Re}_t}{50}\right)^2\right]$
C_μ	0.09	C_2	1.92
f_1	1.0	σ_k	1.0
f_2	$1.0-0.3\exp(-\mathrm{Re}_t^2)$	σ_ε	1.3
C_1	1.44	Re_t	$\rho k^2/\mu\varepsilon$
Pr_t	0.9	Sc_t	1.0

$$\vec{F}_{\text{drag}} = \frac{\pi}{8} d_p^2 C_D \rho_l \left|\vec{u}_p - \vec{u}_l\right| \left(\vec{u}_p - \vec{u}_l\right) \tag{14}$$

where C_D is a dimensionless drag coefficient as a function of particle Reynolds number, according to the approach of Crowe et al. [17], $C_D = \left(1 + 0.15 Re_p^{0.687}\right) 24/Re_p$, $Re_p = \rho_l d_p \left|\vec{u}_p - \vec{u}_l\right| / \mu$, Re_p is particle Reynolds number. $\vec{u}_l$ is instantaneous velocity, which will be described below.

The pressure gradient force can be given as follows:

$$\vec{F}_p = -\frac{\pi}{6} d_p^3 \nabla p \tag{15}$$

The buoyancy force can be expressed as:

$$\vec{F}_b = \frac{\pi}{6} d_p^3 (\rho_l - \rho_p) \vec{g} \tag{16}$$

The virtual mass force, takes in account that an accelerating or decelerating body should accelerate a volume of surrounding fluid equal to one half of the volume a sphere displaces:

$$\vec{F}_{VM} = \frac{\pi}{6} d_p^3 \rho_l C_{VM} \frac{d}{dt} \left(\vec{u}_l - \vec{u}_p\right) \tag{17}$$

where C_{VM} is virtual mass force coefficient, which is set as 0.5 [18].

The stochastic transport of particles (STP) [19] is adopted to incorporate the stochastic effect of turbulent fluctuations on particle. In STP model, velocity fluctuations are based on a Gaussian-distributed random number chosen according to the kinetic energy of the local turbulence. The random number is changed to produce a new instantaneous velocity fluctuation at a frequency equal to the characteristic lifetime of the eddy. The instantaneous velocity is then given by:

$$\begin{aligned} u_{l,i} &= \bar{u}_i + u_i' \\ u_i' &= \xi (2k/3)^{1/2} \end{aligned} \tag{18}$$

where $\bar{u}_i$ is mean velocity component of the fluid flow in direction i, u_i' is component of Gaussian-distributed random velocity fluctuation in direction i.

Computational Procedure

Geometry Model and Numerical Scheme

Geometry Model and Thermophysical Parameters

The DC casting process of Al-4.5 pct Cu alloy is numerically studied in this work, the operation parameters and thermo-physical parameters applied in the simulation are listed in Table 2. In order to enhance the computing efficiency, a two-dimensional model shown in Fig. 1 was used here.

Numerical Scheme

The model was solved in the computational domain shown in Fig. 1 with the appropriate initial conditions, boundary conditions, and thermo-physical parameters in open-source software OpenFOAM [20]. The finite volume method (FVM) was applied to the set of macroscopic transport equations. The large time-step transient solver, PIMPLE (a merged PISO-SIMPLE algorithm), was used to solve the pressure-velocity coupling; this algorithm has shown superior numerical stability in large time-steps calculations as compared to the Pressure Implicit Splitting Operator (PISO) algorithm [21], which is applied in the PIMPLE algorithm to rectify the pressure-velocity correction, while the

Table 2 Operation parameters and thermo-physical parameters

Parameters	Values
Casting speed, m/min	0.09
Ingot diameter, mm	200
Pouring temperature, K	965
Density, kg/m^3	2500
Solid specific heat, J/(kg K)	958
Liquid specific heat, J/(kg K)	1054
Liquid thermal conductivity, W/(m K)	95
Solid thermal conductivity, W/(m K)	180
Thermal expansion coefficient, K^{-1}	1.17×10^{-4}
Liquid viscosity, Pa s	0.0013
Latent heat, J/kg	390,000
Melting point of Al, K	933.5
Liquidus temperature, K	921
Solidus temperature, K	821

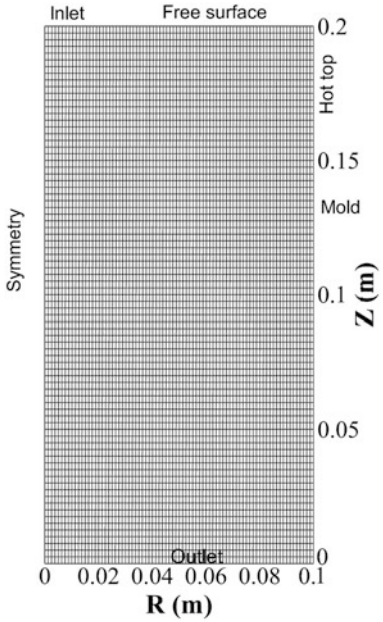

Fig. 1 Geometry model and the corresponding mesh

Semi-Implicit Method for Pressure-Linked equations (SIMPLE) algorithm allowed us to calculate the pressure from velocity components on a grid by coupling Navier–Stokes equations with an iterative procedure. Both numerical stability and efficiency can be achieved with the PIMPLE algorithm. The whole solving process consists of two steps: the transient simulation of the fluid flow and solidification is firstly executed for 160 s, providing an initial condition for the following calculation, which coupled the motion of free-floating crystals with the fluid flow and solidification. The time step was set at 1e−4s in the calculation of particle transport.

Boundary Conditions

The boundary conditions considered applicable to the macrosegregation simulation in continuously cast billet are described as follows.

Free Surface

The free surface was set to be adiabatic wall. The normal gradients of other variables were set to be zero.

Inlet and Outlet

Molten aluminum is poured into the mold through a straight nozzle at a certain flow rate corresponding to the casting speed. The inlet velocity profile was assumed to be flat and determined based on the inlet-outlet mass balance. Thus, boundary conditions of all variables at the inlet can be described as follows:

$$u_x = 0,\ u_y = u_{in} = \frac{4w_b^2}{\pi d_{in}^2} u_c \tag{26}$$

$$T_{in} = T_c \tag{27}$$

where w_b represents the ingot diameter, d_{in} is the diameter of nozzle, and T_c is the pouring temperature. The values of k and ε at the inlet were calculated on the basis of the semi-empirical equations [22]. At outlet, fully developed condition was adopted for the fluid flow, and normal gradients of other variables were set to be zero.

Moving Wall

In the simulation, the ingot surface was treated as a moving wall, and the velocity was set to equal casting speed, and the thermal boundary conditions can be calculated as follows:

$$q_s = h(T_{surf} - T_e) \tag{28}$$

where T_{surf} is the surface temperature of billet, T_e is the environment temperature, and h is the integrative heat transfer coefficient, which can be calculated using the following equations.

In the mold zone, the heat transfer coefficient was treated as a function of solid fraction to take into account the influence of air gap on heat transfer:

$$h = h_{contact}(1 - f_s) + h_{air} \cdot f_s \tag{31}$$

Heat transfer coefficient in the secondary cooling region varies with the change of surface temperature, and the expression of Zhang et al. [23] was applied in the simulation.

Results and Discussion

Solidification

Figure 2 shows the contour plot of predicted liquid fraction, also the isoline with the value of 0.6 (fs = 0.4) is indicated with the black line in the figure. The position of the crater end, shape of mushy zone and the related solidified shell can be clearly identified in the figure. The predicted temperature profiles at different positions of the ingot are shown in Fig. 3. As shown, the temperature in the ingot decreases slowly during early solidification as affected by the adiabatic hot top (0.14–0.20 m). The molten solidifies as soon as reaching the mold region (0.11–0.14 m), wherein the surface temperature decreases rapidly below the solidus temperature. The temperature at the center and quarter changes little in the meantime for the low cooling intensity. After that, the temperature of the whole ingot gradually decreases, and the smallest cooling rate occurs at the centerline.

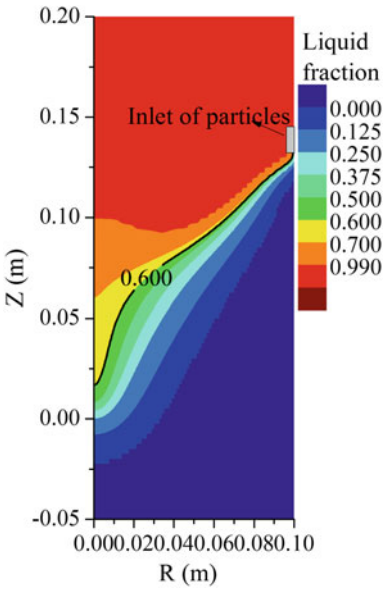

Fig. 2 Contour plot of predicted liquid fraction

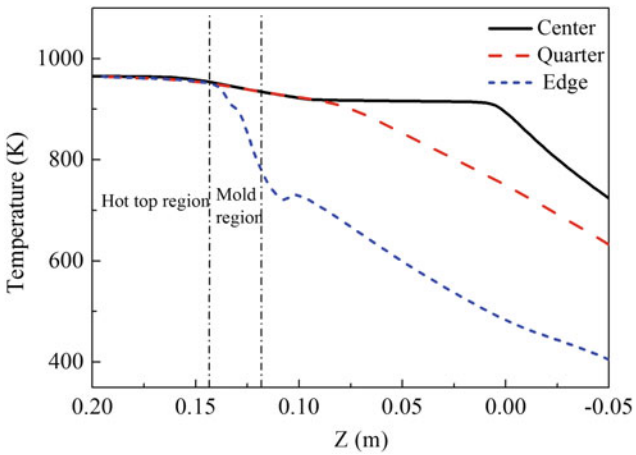

Fig. 3 Predicted temperature profiles at different positions of the ingot

The occurrence of air gap between the ingots, a solidification zone exists at the mold region, where the free-floating crystals will develop and escape from the solidified shell into the liquid and mushy zone. In the present work, the particles are introduced into the ingot from this region, as shown in the figure with the grey frame. The introduction of particles will be clearly indicated in the following figure. The mushy zone gradually develops in the ingot, and the largest mushy zone has been predicted at the central zone in response to the smallest cooling rate. And this will contribute to the growth of crystals in this region.

Motion and Distribution of Free-Floating Crystals

Figure 4 depicts the distribution of the particles (with the size of 130 μm) at different moments from the time particles were introduced: 1, 5, 10, 20, 30, and 50 s. It should be note that the duration time of particle addition is 10 s, and the number of particles is set to be 50 per second. Also, the mushy zone patterns are identified with iso-lines, red line represents the iso-line of 0.99 liquid fractions, and the liquid fraction of 0.01 is given as the black line. The coherency point with the solid fraction of 0.4 (liquid fraction 0.6) is shown in the figure by the orange dashed line. At the time of 1 s, the particles are just introduced into the ingot, and the position of the particle addition can be clearly identified, although the position might not be accurate for the formation of free-floating crystals. The inaccurate position of particles injection, corresponding to small liquid fraction (less than 0.6), leads to the immediate sediment near the ingot surface. A number of particles float into the liquid as affected by the turbulent fluctuation and buoyancy. In fact, most of these floating crystals will be re-melted for the high temperature in this region, and the others will plunge into the slurry zone with the fluid flow.

To investigate the influence of particle size on their distribution, the particles with 8 different diameters (10, 40, 70, 100, 130, 200, 350, and 500 μm) are uniformly introduced into the ingot at the same time. The predicted distribution of the particles with different sizes is shown in Fig. 5, and the computing time is 50 s. The red particle represents the smallest size (10 μm), and the largest is identified by blue ones (500 μm). As shown in the figure, most of the blue particles are predicted to be in the completely solidified region (below the black line), and the red ones are randomly distributed in the liquid zone (above the red line). The predicted distribution indicates that the large particles are more prone to go down into the mushy zone and captured by the solidified shell. While the particles with small diameters tend to float into the liquid and slurry zones affected by the turbulent fluctuation and buoyancy. The effect of size on distribution can be more clearly identified from Fig. 6, which illustrates the distribution of particles with three different sizes (10, 130, 200, and 350 μm). As shown, with the same computing time and particle number, the ratio of free-floating particles of 350 μm in the liquid obviously less than that with the size of 10 μm. These findings suggest that large free-floating crystals tend to be captured as soon as their formation, while small ones are prone to float into the region with high temperatures. And all of them hardly arrive at the center of ingots, only the free-floating crystals with

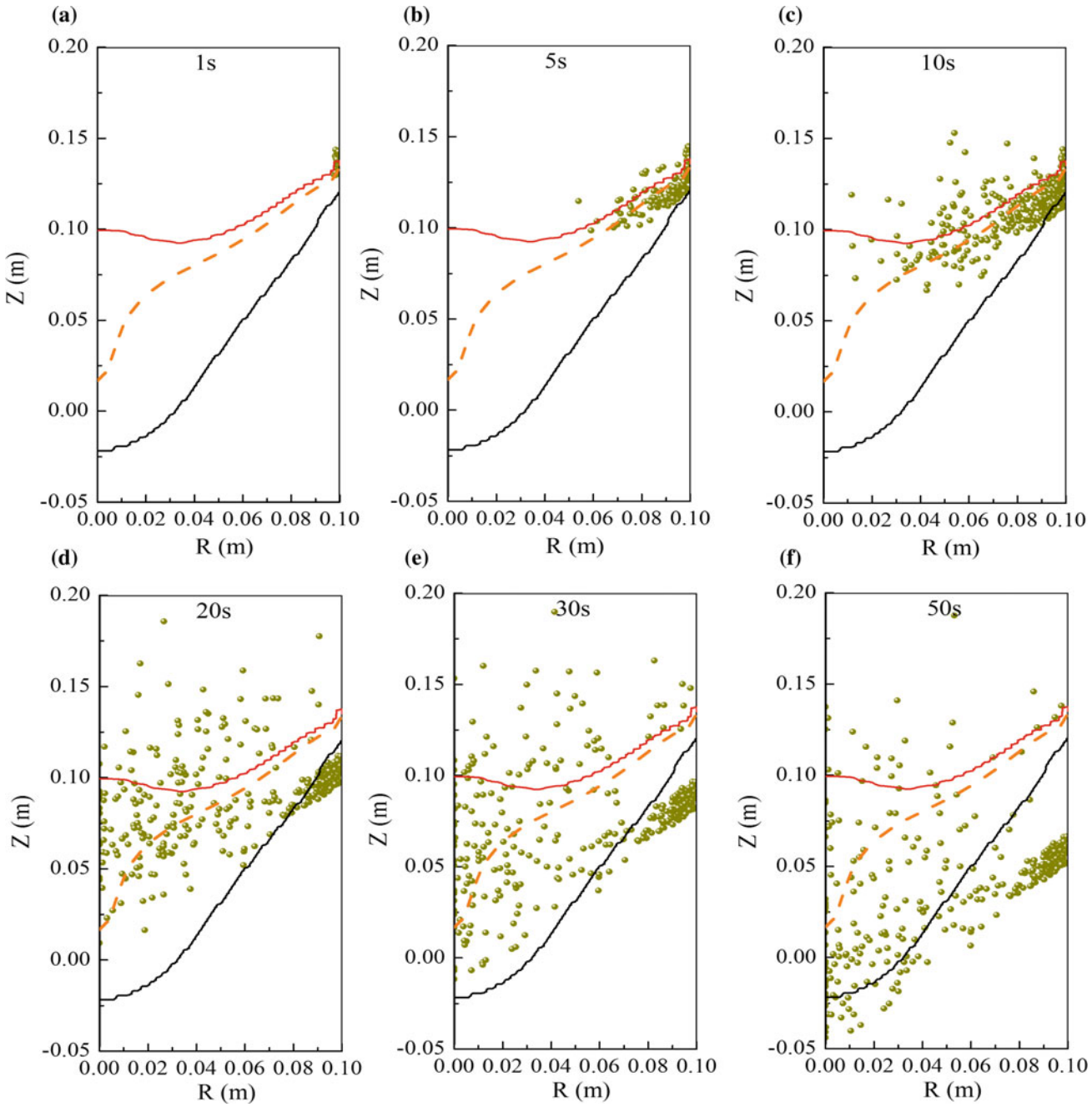

Fig. 4 Distribution of the particles at different computing time

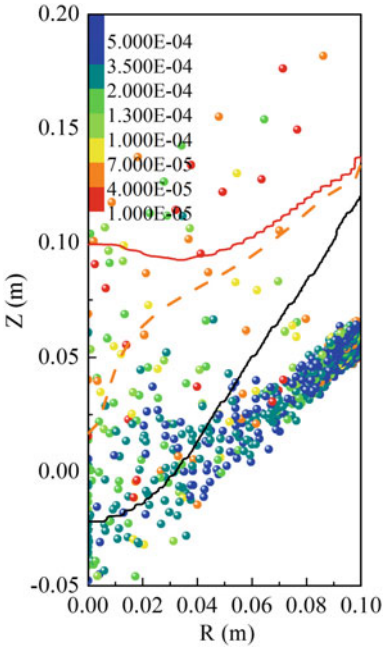

Fig. 5 Distribution of the particles with different diameters

moderate sizes can move to the ingot center along the nearby region of slurry.

Conclusions

A mathematic model coupling the fluid flow, solidification, and transport of free-floating crystals is developed to investigate the motion and distribution of free-floating crystals during DC casting process of aluminum alloys. The liquid fraction patterns and characteristics of solidification are given in this work. When the particles are introduced, a number of them float into the liquid as affected by the turbulent fluctuation and buoyancy, while the others go down into the mushy zone and are captured further by the solidified shell. The results of different diameters show that large particles are more prone to be captured by the solidified shell, and small ones tend to be floating in the liquid and then re-melted. This indicates that only the free-floating crystals with moderate sizes can move to the ingot center along the nearby region of slurry and affect the formation of centerline segregation.

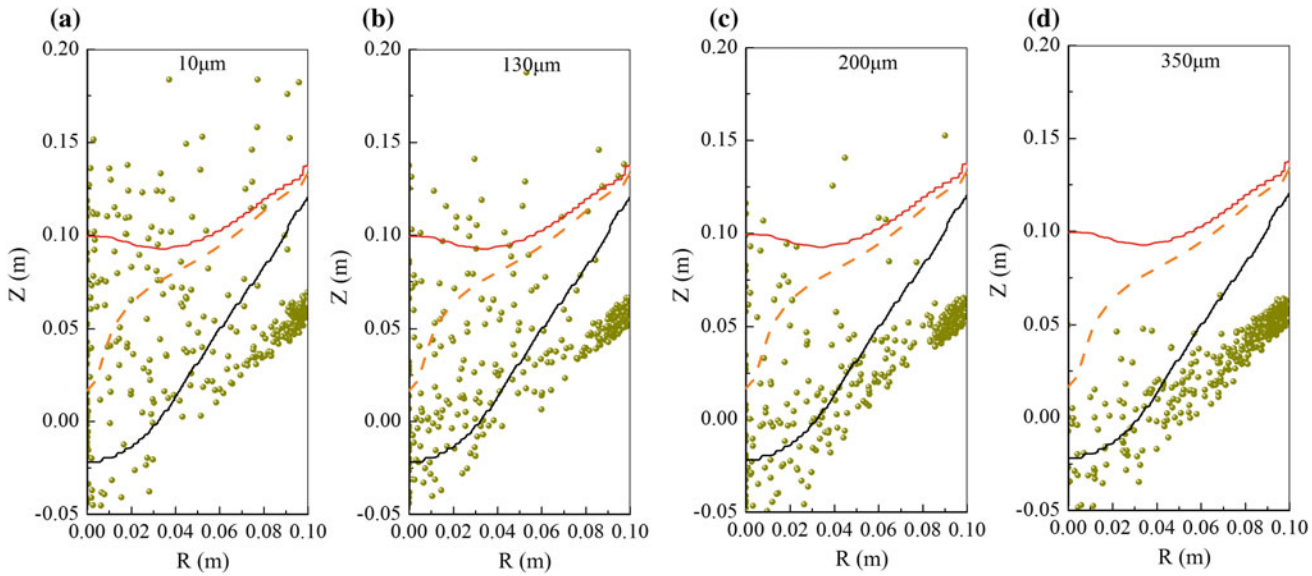

Fig. 6 Comparison of the distribution of particles with three different sizes

Acknowledgements This research was financially supported by Postdoctoral Science Foundation of Jiangsu Province of China.

References

1. Eskin, D.G. (2008) Physical metallurgy of direct chill casting of aluminum alloys. CRC press.
2. Suyitno, E.D., V. Savran, L. Katgerman (2004) Effects of alloy composition and casting speed on structure formation and hot tearing during direct-chill casting of Al-Cu alloys. Metall. Mater. Trans. A. 11: 3551–3561.
3. Eskin, D.G., V.I. Savran, L. Katgerman (2005) Effects of melt temperature and casting speed on the structure and defect formation during direct-chill casting of an Al-Cu alloy. Metall. Mater. Trans. A. 7: 1965–1976.
4. Nadella, R., D. Eskin, L. Katgerman (2008) Effect of Grain Refinement on Structure Evolution, "Floating" Crystals, and Centerline Macrosegregation in Direct-Chill Cast AA2024 Alloy Billets. Metall. Mater. Trans. A. 2: 450–461.
5. Vreeman, C.J., M.J.M. Krane, F.P. Incropera (2000) The effect of free-floating crystals and convection on macrosegregation in direct chill cast aluminum alloys: Part I: model development. Int. J. Heat Mass Tran. 5: 677–686.
6. Vreeman, C.J., F.P. Incropera (2000) The effect of free-floating crystals and convection on macrosegregation in direct chill cast aluminum alloys: Part II: predictions for Al–Cu and Al–Mg alloys. Int. J. Heat Mass Tran. 5: 687–704.
7. Ni, J., F.P. Incropera (1995) Extension of the continuum model for transport phenomena occurring during metal alloy solidification—I. The conservation equations. Int. J. Heat Mass Tran. 7: 1271–1284.
8. Ni, J., F.P. Incropera (1995) Extension of the continuum model for transport phenomena occurring during metal alloy solidification-II. Microscopic considerations. Int. J. Heat Mass Tran. 7: 1285–1296.
9. Krane, M.J.M. (2004) Macrosegregation development during solidification of a multicomponent alloy with free-floating solid particles. Appl. Math. Model. 1: 95–107.
10. Lesoult, G. (2005) Macrosegregation in steel strands and ingots: Characterisation, formation and consequences. Mater. Sci. Eng. A. 413:19–29.
11. Reddy, A., N.C. Beckermann (1997) Modeling of macrosegregation due to thermosolutal convection and contraction-driven flow in direct chill continuous casting of an Al-Cu round ingot. Metall. Mater. Trans. B. 3: 479–489.
12. Turchin, A.N., D.G. Eskin, L. Katgerman (2007) Solidification under Forced-Flow Conditions in a Shallow Cavity. Metall. Mate. Trans. A. 6: 1317–1329.
13. Eskin, D., et al (2007) Reprogrammable FPLA with Universal Test Set. in Proc. Of the 5th Dec. Int. Conf. on Solid. Proc.
14. Prescott, P., F. Incropera (1995) The effect of turbulence on solidification of a binary metal alloy with electromagnetic stirring. Jour. Heat Trans. 3: 716–724.
15. Mathur, A., S. He (2013) Performance and implementation of the Launder–Sharma low-Reynolds number turbulence model. Comput. Fluids. 79: 134–139.
16. Clyne, T., W. Kurz (1981) Solute redistribution during solidification with rapid solid state diffusion. Metall. Trans. A. 6: 965–971.
17. Schwarzkopf, J.D., et al. (20110 Multiphase flows with droplets and particles.CRC press.
18. Liu, Z., L. Li, B. Li (2016) Large eddy simulation of transient flow and inclusions transport in continuous casting mold under different electromagnetic brakes. JOM. 8: 2180–2190.
19. Baxter, L., P. Smith (1993) Turbulent dispersion of particles: the STP model. Energ. Fuel. 6: 852–859.
20. Jasak, H., A. Jemcov, and Z. Tukovic (2007) OpenFOAM: A C++ library for complex physics simulations. in International workshop on coupled methods in numerical dynamics. IUC Dubrovnik, Croatia.
21. Kang, K., H. Ryou (2010) Computation of solidification and melting using the Piso algorithm. Numer. Heat Tr. B. Fund. 2: 179–194.
22. Lai, K. (1986) Mathematical modeling of flows in large tundish systems in steelmaking. Metall. Trans. B. 3: 449–459.
23. Zhang, H.T. (2007) Coupled modeling of electromagnetic field, fluid flow, heat transfer and solidification during low frequency electromagnetic casting of 7XXX aluminum alloys: Part 1: development of a mathematical model and comparison with experimental results. Mater. Sci. Eng. A. 1–2: 189–203.